Identification of a Dynamic Equivalent of an Active Distribution Network from Monte-Carlo Simulations

Gilles Chaspierre
Dept. of Elec. Eng. and Comp. Science
University of Liège, Belgium
g.chaspierre@uliege.be

Guillaume Denis Patrick Panciatici
Research & Development Dept.
RTE, Paris La Défense, France
patrick.panciatici@rte-france.com

Thierry Van Cutsem
Fund for Scientific Research (FNRS)
University of Liège, Belgium
t.vancutsem@uliege.be

***Abstract*—This paper deals with the derivation of a dynamic equivalent of a distribution system for use in (phasor-mode) dynamic simulations of large disturbances in the transmission system. The original, unreduced system hosts inverter-based generators such as photovoltaic units or full-converter wind turbines. The individual behaviour of inverter-based generators and loads is assumed to be reasonably well captured by a parameterized model, but the values of its parameters are uncertain. Monte-Carlo simulations involving random variations of those parameters are performed, yielding a set of dynamic responses to a given large disturbance. The equivalent is of the "grey-box" type and its parameters are tuned in the least-square sense to have its response falling in time-varying confidence intervals obtained from the 5-th and the 95-th percentiles of the distribution of dynamic responses. Simulations results are reported on a variant of the CIGRE Medium-Voltage Distribution Network Benchmark.**

***Index Terms*—active distribution networks, inverter-based generators, Monte-Carlo simulations, short-term dynamics, model reduction, dynamic equivalents**

I. Introduction

Distribution grids are expected to host more and more distributed generation. Most of these generators are connected to the grid through an electronic interface which will significantly change the dynamics of distribution grids. It becomes important to have proper models of such Active Distribution Networks (ADNs) in order to account for their contributions in power system dynamic studies.

For transmission system operators, a unique model of both transmission and distribution systems is not only impractical, but would also entail data confidentiality issues. Indeed, while the Distribution System Operator (DSO) is usually entitled to collect data about the connected equipment, sharing this information with the Transmission System Operator (TSO) may raise legal issues.

Furthermore, it makes sense for DSOs to process the data of their own systems and transmit to the TSO reduced, "anonymized" models of much lower complexity than the original, unreduced model they have assembled. Those "equivalents" are intended to be incorporated to the transmission system model for use by the TSO in dynamic security assessment studies. While such equivalents are free from the aforementioned problems, on the other hand, they should be accurate enough for TSO studies.

The dynamic equivalent considered in this work is of the "grey-box" type, as defined and recommended in [1] and [2].

For DSOs, one major issue when setting up a detailed ADN model is the uncertainty affecting the behaviour of its components. Their dynamic models involve parameters which are not known accurately. In this work, it is assumed that the dynamic behaviour of individual Inverter-Based Generators (IBGs) and loads can be reasonably well captured by parameterized models, but their parameters are uncertain.

A well-known approach to deal with such uncertainty consists of performing Monte-Carlo (MC) simulations [3], involving in this case random variations of the model parameters. Thus, for a given disturbance and an initial operating point, a set of randomized time responses is generated [4].

Several ways of exploiting the MC simulations can be thought of. A first one consists of extracting one representative instance of the detailed, unreduced model [5] and tuning the parameters of the equivalent to make its response match that representative evolution as closely as possible. This approach, however, does not account for the dispersion of the dynamic responses revealed by the MC simulations. If there is a large dispersion, there is no point in attempting to make the reduced-order model fit closely one particular response out of the whole set. Instead, it is sufficient that its response falls into (time-varying) confidence intervals derived from the distribution of dynamic responses.

The rest of the paper is organized as follows. The method to determine the above mentioned confidence intervals is detailed in Section II. In Section III, the identification of the equivalent is described. The respective IBG and load models are outlined in Section IV. The test system and the simulations results are presented in Section V, while concluding remarks are offered in Section VI.

II. Assessing the unreduced system with Monte-Carlo simulations

A. Generating Monte-Carlo simulations

The procedure to generate the MC simulations is detailed in [5]. It involves random variations of the parameters of the unreduced ADN model. In this paper, the parameters are uniformly distributed in realistically chosen intervals. Note that they are randomized from one MC simulation to another, but also from one bus to another inside the same MC simulation.

The dynamic simulations involve responses to large disturbances (typically faults) taking place in the transmission system. The variables of interest are the active and reactive powers entering the ADN. Several disturbances, mainly voltage dips, are applied by a time-varying voltage source replacing the external system, and the time responses of the powers are collected for the various instances of the ADN model.

B. Choosing the number of Monte-Carlo simulations

The number of MC simulations must be large enough for the randomly drawn sample to be representative, but it should be limited to keep the computational burden reasonable. It is thus desirable to stop generating randomized responses once sufficient information is contained in the sample.

The approach consists of increasing the sample until the average power response does no longer vary significantly. Denoting by k the discrete time ($k = 1, \ldots, N$) and by $\mathbf{p}_i$ the i-th randomly drawn vector of parameters, the detailed procedure is as follows [5]:

1) initialize: $s = s_o$, $g = 0$;
2) draw at random an initial set of s_o parameter vectors $(\boldsymbol{p}_1, \ldots, \boldsymbol{p}_{s_o})$;
3) for each parameter vector, simulate the ADN dynamic response to the disturbance;
4) compute the average power responses $\bar{P}(s_o, j, k)$ and $\bar{Q}(s_o, j, k)$;
5) generate a new random parameter vector $\boldsymbol{p}_{s+1}$, and simulate the correspondng ADN response to the disturbance;
6) compute the new average power responses $\bar{P}(s+1, j, k)$ and $\bar{Q}(s+1, j, k)$;
7) compare them with the previous averages by computing the Euclidean distance:

$$\lambda = \sqrt{\lambda_P^2 + \lambda_Q^2} \tag{1}$$

where:

$$\lambda_P^2 = \frac{1}{N} \sum_{k=1}^{N} \left[\bar{P}(s+1, j, k) - \bar{P}(s, j, k)\right]^2 \tag{2}$$

$$\lambda_Q^2 = \frac{1}{N} \sum_{k=1}^{N} \left[\bar{Q}(s+1, j, k) - \bar{Q}(s, j, k)\right]^2; \tag{3}$$

8) if $\lambda \leq \delta$ then $g \to g+1$; else $g = 0$;
9) if $g = g_{max}$ then stop; else $s \to s+1$, go to Step 5.

As it can be seen, the procedure starts by performing a set of s_o MC simulations. Simulations are added one by one until λ has remained smaller than the tolerance δ over the last g_{max} simulations. With this proposed stopping criterion, randomizing more parameters does not necessarily increase the computational burden [5].

C. Extracting the confidence intervals

As mentioned in the Introduction, time-varying confidence intervals are obtained from the distribution of dynamic responses. At a given time k, the lower and upper bounds of the active (resp. reactive) power confidence interval are obtained as percentiles of the distribution of values taken by the active (resp. reactive) power at that time [6]. Time-varying confidence intervals are obtained by assembling the intervals determined at all times k. In this work, the 5-th and 95-th percentiles have been considered. Their use is explained in the next section.

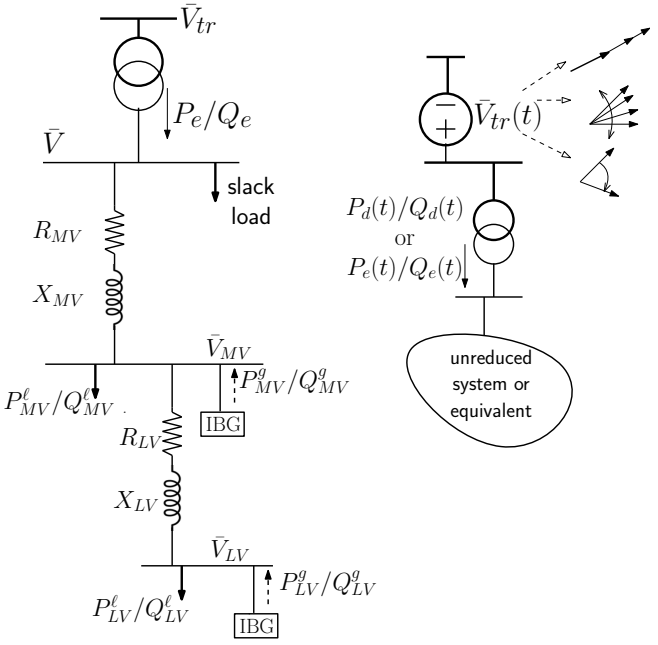

Fig. 1. Structure of the equivalent and training signals

III. Identification of the ADN equivalent

A. Structure of the equivalent

The structure of the equivalent is shown in the left part of Fig. 1. The originally distributed IBGs (resp. loads) are aggregated into two lumped, equivalent IBGs (resp. loads). They are differentiated by voltage levels, to separate medium- and low-voltage devices, assumed to have different technical characteristics. The aggregated components are placed behind equivalent impedances accounting for the network effects. Namely, R_{MV} and X_{MV} account for the medium-voltage distribution grid, while R_{LV} and X_{LV} account for the low-voltage networks.

The main substation transformer is modeled explicitly.

B. Identifying the parameters of the equivalent

In order to be valid for large disturbances, the equivalent should be derived from multiple "training" scenarios involving representative disturbances. Such scenarios are obtained by replacing the transmission system with a time-varying voltage source $\bar{V}_{tr}(t)$, shown in the right part of Fig. 1. $\bar{V}_{tr}(t)$ should involve typical variations of the corresponding voltage, such as variations of amplitude, phase jumps and frequency.

The $\bar{V}_{tr}(t)$ signals are applied to both the unreduced ADN model and the equivalent. The outputs of interest are the active and reactive powers entering the distribution grid. $P_d(t)$ and

$Q_d(t)$ account for the active and reactive power responses of the detailed ADN, respectively.

The parameters of the equivalent are grouped in the $\boldsymbol{\theta}$ vector.

Let m be the number of training signals. For the j-th signal $(j = 1, \ldots, m)$, let us denote by:

$P_e(\boldsymbol{\theta}, j, k)$	the discrete-time evolution of the active power entering the equivalent system (see Fig. 1) ;
$Q_e(\boldsymbol{\theta}, j, k)$	the corresponding evolution of reactive power;
$P_l(j, k)$	the discrete-time evolution of the lower bound of the confidence interval of active power (determined as described in Section II-C);
$Q_l(j, k)$	the corresponding evolution of reactive power;
$P_u(j, k)$	the discrete-time evolution of the upper bound of the confidence interval of active power;
$Q_u(j, k)$	the corresponding evolution of reactive power;

where k refers to the discrete times used by the time-simulation solver $(k = 1, \ldots, N)$. The same time instants are considered for both the unreduced and the equivalent system; if needed, interpolation is used to make the time instants coincide.

$\boldsymbol{\theta}$ is adjusted to minimize the objective function:

$$\varepsilon(\boldsymbol{\theta}) = \sqrt{\varepsilon_P(\boldsymbol{\theta}) + w\, \varepsilon_Q(\boldsymbol{\theta})} \quad (4)$$

$$\text{with} \quad \varepsilon_P(\boldsymbol{\theta}) = \frac{1}{m} \sum_{j=1}^{m} \sum_{k=1}^{N} \varepsilon_P(j, k) \quad (5)$$

$$\varepsilon_Q(\boldsymbol{\theta}) = \frac{1}{m} \sum_{j=1}^{m} \sum_{k=1}^{N} \varepsilon_Q(j, k) \quad (6)$$

where the errors at time k are given by the barrier functions :

$$\varepsilon_P(j,k) = \begin{cases} [P_l(j,k) - P_e(\boldsymbol{\theta},j,k)]^2 & \text{if } P_e(\boldsymbol{\theta},j,k) < P_l(j,k) \\ [P_u(j,k) - P_e(\boldsymbol{\theta},j,k)]^2 & \text{if } P_e(\boldsymbol{\theta},j,k) > P_u(j,k) \\ 0 & \text{otherwise,} \end{cases}$$

$$\varepsilon_Q(j,k) = \begin{cases} [Q_l(j,k) - Q_e(\boldsymbol{\theta},j,k)]^2 & \text{if } Q_e(\boldsymbol{\theta},j,k) < Q_l(j,k) \\ [Q_u(j,k) - Q_e(\boldsymbol{\theta},j,k)]^2 & \text{if } Q_e(\boldsymbol{\theta},j,k) > Q_u(j,k) \\ 0 & \text{otherwise,} \end{cases}$$

under the constraints :

$$\boldsymbol{\theta}^L \leq \boldsymbol{\theta} \leq \boldsymbol{\theta}^U. \quad (7)$$

In Eq. (4), w is a weight assigned to the reactive power responses with respect to the active ones. The bounds $\boldsymbol{\theta}^L$ and $\boldsymbol{\theta}^U$ keep $\boldsymbol{\theta}$ in realistic ranges of values.

The barrier function is illustrated for the active power in Fig 2. The idea is to force the dynamic responses of the equivalent to fall in the confidence intervals $[P_l(j,k)\ P_u(j,k)]$ and $[Q_l(j,k)\ Q_u(j,k)]$, for all training disturbances. If this was achieved, the objective function in (4) would reach a zero value. Further optimization is not sought considering the uncertainty on the response of the unreduced, reference model.

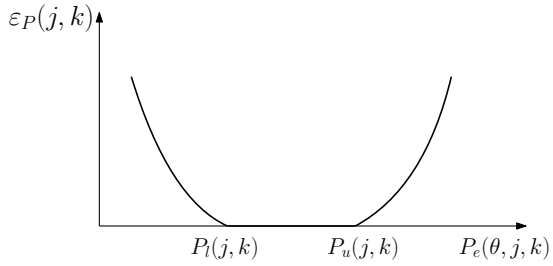

Fig. 2. Barrier function used in the identification of the equivalent

At this stage of the research, a meta-heuristic optimization method has been used, namely a variant of the Differential Evolution (DE) algorithm [7] to solve the above minimization problem. Please refer to [8] for additional information.

C. Initializing the equivalent

With reference to Fig. 1, the initial active and reactive powers P^{ℓ}_{MV} and Q^{ℓ}_{MV} (resp. P^{g}_{MV} and Q^{g}_{MV}) are obtained by aggregating the consumptions of all dispersed loads (resp. the productions of all dispersed IBGs) connected to MV buses in the unreduced model. The same applies to loads and IBGs connected at LV level and aggregated at the LV equivalent bus, yielding $P^{\ell}_{LV}, Q^{\ell}_{LV}, P^{g}_{LV}$ and Q^{g}_{LV}.

Since the resistances R_{MV}, R_{LV} and reactances X_{MV}, X_{LV} are components of the $\boldsymbol{\theta}$ vector to identify, the losses in the two equivalent impedances change from one value of $\boldsymbol{\theta}$ to another. On the other hand, the initial values of the active and reactive powers entering the distribution grid must remain at the same (measured or forecasted) values. Hence, to satisfy the power balance, a "slack" load is added, as shown in Fig. 1. This load is usually small.

IV. IBG and load models

A. Load model in the unreduced system

As sketched in Fig. 3, each load is split into an equivalent induction motor with third-order model. That motor consumes initially a fraction f of the load active power. The rest of the load is modeled with a static exponential model, as shown in the figure.

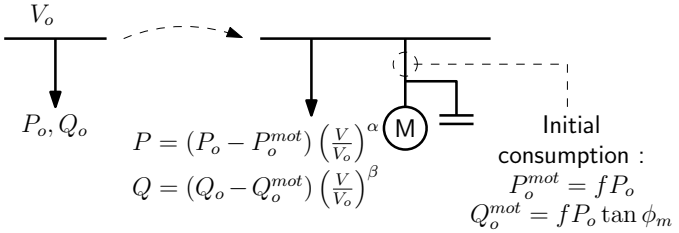

Fig. 3. Load composition. P_o (resp. Q_o) stands for either P^{ℓ}_{MV} or P^{ℓ}_{LV}, and Q_o for either Q^{ℓ}_{MV} or Q^{ℓ}_{LV}

B. Load model in the equivalent

The aggregated load model in the equivalent is identical to the load model in the unreduced system.

C. IBG model in the unreduced system

Instead of focusing on internal components, the model reproduces the IBG response to terminal voltage changes in accordance with grid codes [9]–[11]. The main control functions are described hereafter. They involve non-linearities or discontinuous control. More detailed block diagrams and additional information can be found in Refs. [8] and [12].

1) Phase Locked Loop (PLL): The PLL dynamics is represented in some detail, as shown in Fig. 4. It determines the phase angle θ of the terminal voltage phasor. The magnitude of the current phasor and its phase shift with respect to the voltage phasor are adjusted in order to generate the required active and reactive currents.

In Fig. 4, v_x and v_y (resp. i_x and i_y) are the projections on reference axes (x, y) of the phasor of the terminal voltage (resp. the current injected into the grid). The gains k_{Ipll} and k_{Ppll} determine the PLL response time, while V_{PLL} is the voltage threshold below which it is blocked. T_m is a time constant accounting for the measurement while i_P and i_Q are the active and reactive current commands from the control blocks of the inverter, respectively. T_m has been set to 20 ms for large-scaled IBGs (e.g. industrial installations) and to 30 ms for small IBGs (e.g. residential rooftop photovoltaic units).

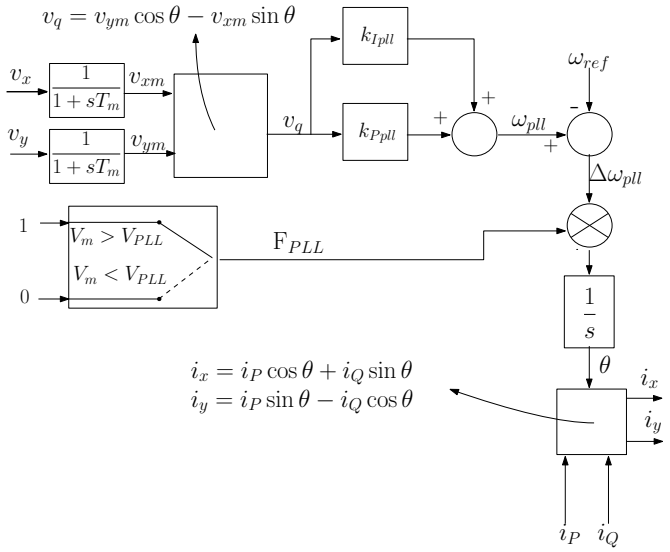

Fig. 4. Block diagram of the PLL

2) Low Voltage Ride-Through (LVRT): LVRT capability is an important feature of IBGs, requiring them to remain connected to the grid during a disturbance as long as the voltage is above a reference curve, as shown in Fig. 5. If the terminal voltage of an IBG falls below the reference curve, the unit is allowed to disconnect from the grid.

3) Reactive current injection: In low voltage conditions IBGs (with a nominal power above some value) are requested to inject reactive current to support their terminal voltages. The injected current varies linearly with the measured voltage magnitude, as shown in Fig. 6. I_{nom} is the nominal current of the inverter and V_m the voltage magnitude measured at its terminal. V_{S1} is the voltage at which the inverter starts injecting reactive current in the grid while m is in the range [0 1]. Typically, $m = 0$, $V_{S1} = 0.9$ pu, and $2 \leq k_{RCI} \leq 6$ as suggested in [11].

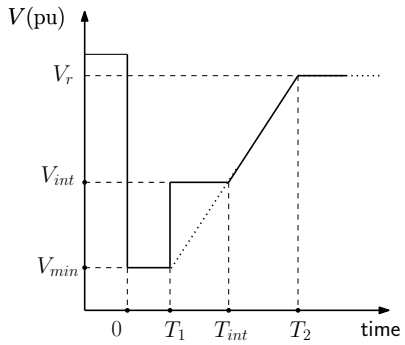

Fig. 5. LVRT characteristic (fault occurring at $t = 0$)

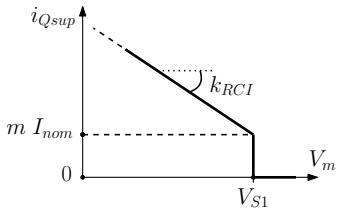

Fig. 6. Reactive current injection characteristic

4) Active power recovery: When an IBG is called to support the grid voltage, it may happen that its active current is reduced to leave room for its reactive counterpart without exceeding the inverter current limit. Once the voltage has recovered to normal values, the IBG recovers its active current. This cannot take place too rapidly but it should not take too much time either, to avoid long-lasting power imbalances. Some grid codes (e.g. [11]) specify a range of allowed values for the rate of recovery of the active current.

D. IBG model in the equivalent

The model of the aggregated IBG in the equivalent includes all the features presented in the previous sub-section. In addition, it can reproduce the tripping of some of the individual IBGs it replaces. The main issue is that the equivalent IBG has a single terminal voltage while the individual IBG voltages differ from one bus to another throughout the distribution network. This issue has been tackled by providing the equivalent IBGs with a "partial tripping" feature. The latter consists of multiplying the output current by a factor $f_1 f_2 f_3$ with $0 \leq f_1, f_2, f_3 \leq 1$, where f_1, f_2 and f_3 relate respectively to the time intervals $[0\ T_1]$, $[T_1\ T_{int}]$ and $[T_{int}\ T_2]$ of the LVRT curve in Fig. 5 [8].

E. Total number of parameters to identify

The $\boldsymbol{\theta}$ vector has a total of 40 components to identify. A preliminary sensitivity analysis identified 11 parameters with small or negligible influence on the model responses. The remaining parameters include :

- for the IBGs: the nominal apparent power, the inverter main time constant, the parameters of the LVRT curve (see Fig. 5), the k_{RCI} slope and the V_{S1} threshold (see Fig. 6), the active current recovery rate r, and parameters involved in the partial tripping;
- for the loads: the fraction f, the exponent α, the initial power factor $\cos\phi_m$ (see Fig. 3) and some parameters of the motor such as the load factor and the inertia constant;
- for the network: $R_{MV}, X_{MV}, R_{LV}, X_{LV}$ (see Fig. 1).

V. Simulation results

A. Test system

The simulations were performed on a variant of the CIGRE Medium-Voltage Distribution Network Benchmark [13], at a single operating point. Its one-line diagram is shown in Fig. 7. The system feeds different categories of loads : residential loads with a consumption of 16.24 MW and industrial loads with a consumption of 4.3 MW.

The system also hosts dispersed IBGs of two types. The large-scale IBGs account for 2.67 MW. They have fault-ride-through and reactive current injection capabilities. Some of them instantaneously trip when their measured terminal voltage falls below the reference curve, while the others remain connected. Whether an IBG falls in the first or the second category changes randomly from one MC simulation to another. For the second category, the V_{min} threshold (see Fig. 5) is set to zero.

The small-scale IBGs corresponding to residential rooftop photovoltaic panels account for 180 kW of production. They have no fault-ride-through nor reactive current injection capability. The load and IBG parameters have been randomized from one bus to another within realistic ranges of values in order to add diversity in the system. Specifically, the industrial (resp. residential) loads involve "large" (resp."small") motors with parameters randomized around the values given in [14].

B. Disturbances

The disturbances considered are voltage dips, typically caused by faults, and applied at the transmission side of the main transformer. They are characterized by a duration ΔT and a depth ΔV, as shown in Fig. 8. The values of ΔT and ΔV are given in the same figure for the various disturbances considered in this paper. $\Delta T = 0.10$ s corresponds to faults cleared by primary protections, and $\Delta T = 0.25$ s to faults cleared by back-up protections.

Simulations were performed with RAMSES, a software for time simulation in phasor mode, developed at the University of Liège [15]. The default time step size is 0.01 s, which leads to $N \simeq 300$.

C. Results of Monte-Carlo simulations

The procedure of Section II-B with $s_o = 100$ initial simulations, a tolerance $\delta = 0.05$ MVA and $g_{max} = 10$ led to generate $s = 347$ randomized responses to each of the disturbances.

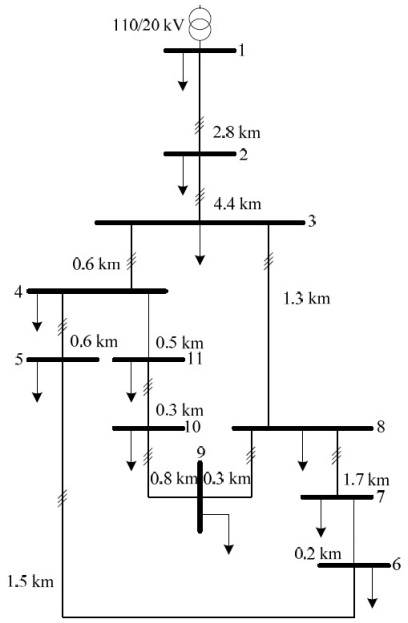

Fig. 7. One-line diagram of CIGRE Medium-Voltage Distribution Network

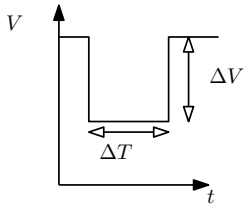

disturb. No	ΔV (pu)	ΔT (s)
1	0.2	0.10
2	0.2	0.25
3	0.3	0.10
4	0.3	0.25
5	0.4	0.10
6	0.4	0.25
7	0.5	0.10
8	0.5	0.25
9	0.6	0.10
10	0.6	0.25
11	0.7	0.10
12	0.7	0.25
13	0.8	0.1
14	0.8	0.25

Fig. 8. Disturbances considered in the simulations

As an illustration, Figs. 9 and 10 show the 347 time evolutions of respectively the active and reactive powers, received by the distribution grid at bus 1 in response to disturbance No 8. Note that all responses correspond to the same operating point; thus, all curves start from the same value. The corresponding curves for disturbance No 14 are given in Figs. 11 and 12.

Those four figures show a sharp increase of active and reactive power immediately after fault clearing. The first reason is that motors draw additional power when re-accelerating after fault clearing. The second reason is that, during the fault, the active currents of large-scale IBGs have been reduced, if not canceled, owing to the priority given to reactive currents for voltage support. This leads to higher active power imports for a short period of time.

For each disturbance, the 5-th and 95-th percentiles were

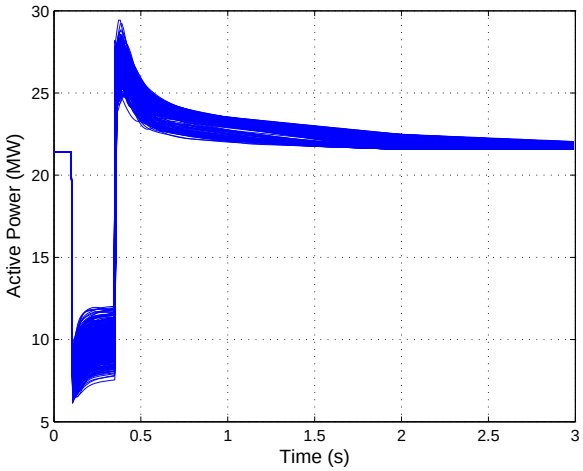

Fig. 9. MC simulations: 347 active power responses to disturbance No 8

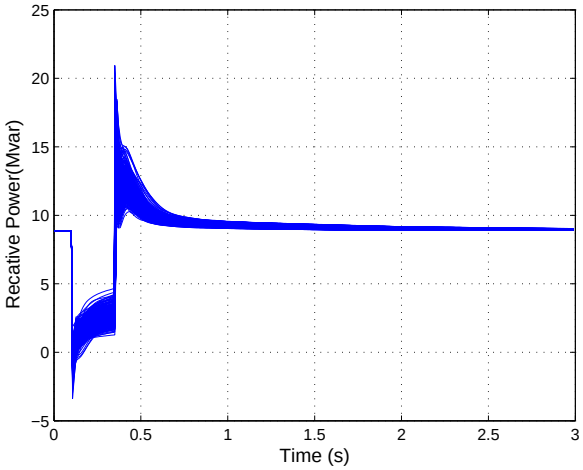

Fig. 10. MC simulations: 347 reactive power responses to disturbance No 8

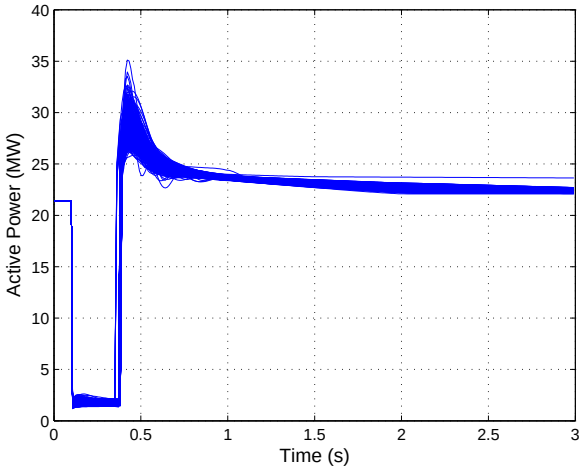

Fig. 11. MC simulations: 347 active power responses to disturbance No 14

extracted using the *prctile* function of MATLAB.

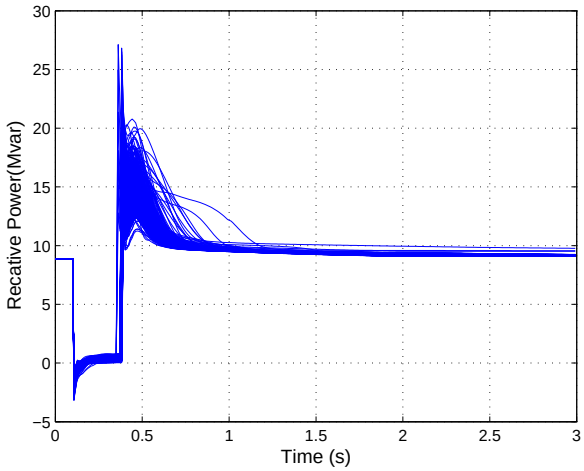

Fig. 12. MC simulations: 347 reactive power responses to disturbance No 14

D. Results of training

The equivalent was trained on the most severe scenarios, namely disturbances No 7 to 14 in Fig 8. It is important to train the equivalent on several disturbances with different severities, in order to avoid "overfitting" one particular scenario.

The optimization problem of Section III-B has been solved with $w = 1$, using the DE algorithm. After 200 iterations, the error $\varepsilon(\boldsymbol{\theta})$ was brought below 3 MVA. This nonzero value indicates that some points of some responses still fall outside the time-varying confidence intervals. Nevertheless, the accuracy is good enough, as shown in the following figures.

Figures 13 and 14 compares the time evolution of, respectively, the active and reactive power responses of the reduced system with the time-varying confidence intervals. They relate to the trained disturbance No 8. The corresponding plots for the trained disturbance No 14 are given in Figs. 15 and 16. For the active power response, it is observed that the final value is slightly larger that the initial one. This corresponds to the tripping of the residential IGBs (without fault-ride-through capability), which the equivalent model is able to reproduce.

Furthermore, the figures show that the responses of the equivalent fall within the time-varying confidence intervals at almost all time steps, as expected from the small final value of $\varepsilon(\boldsymbol{\theta})$. The bounds are slightly exceeded when the (non-tripped) IBGs are ramping up and recovering their initial active power. This is a challenging issue. In the detailed system, this active power recovery is shared by multiple IBGs, while in the equivalent it is assigned to a single IBG. The active current recovery rate r, included in $\boldsymbol{\theta}$, is optimized to fit the various training scenarios in the best possible way.

E. Results of validation

Disturbances No 1 to 6 were used to check that the equivalent is accurate in scenarios not considered when identifying $\boldsymbol{\theta}$ and, i.e. it does not "overfit" the training scenarios.

Figures 17 to 20 compare the time evolutions of, respectively, the active and reactive power responses of the reduced system with the confidence interval obtained from

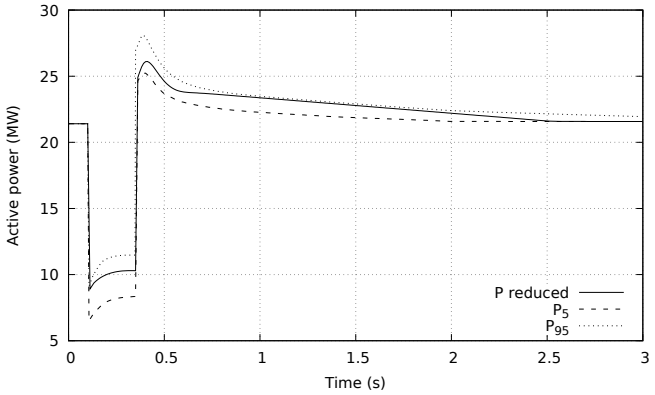

Fig. 13. Trained disturbance No 8: active power response of the equivalent compared to the time-varying confidence interval (P_5, P_{95})

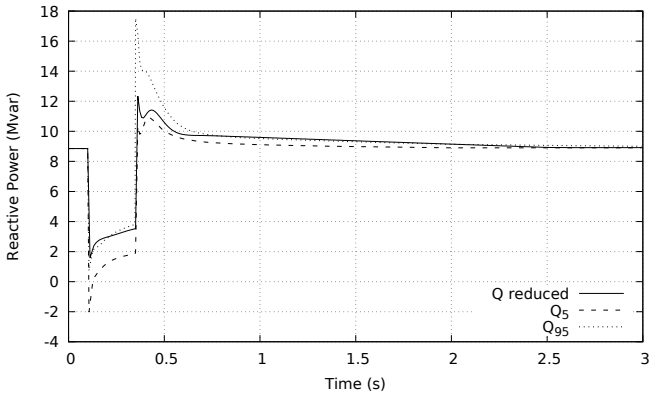

Fig. 14. Trained disturbance No 8: reactive power response of the reduced system compared to the time-varying confidence interval (Q_5, Q_{95})

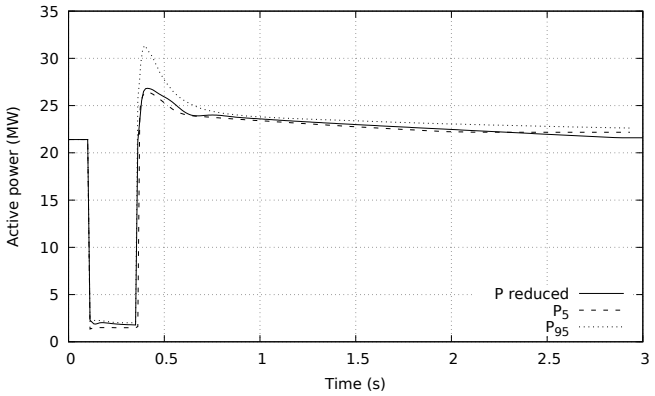

Fig. 15. Trained disturbance No 14: active power response of the reduced system compared to the time-varying confidence interval (P_5, P_{95})

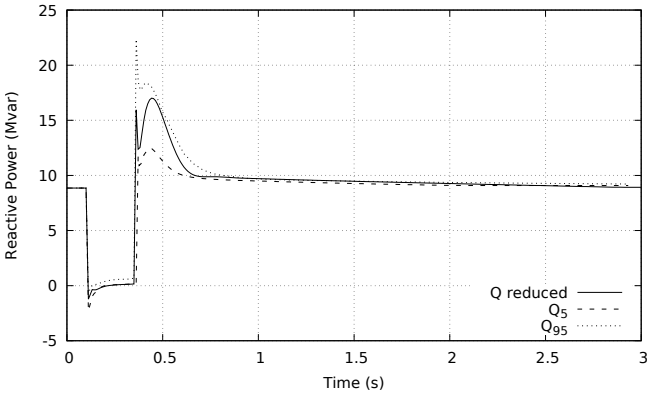

Fig. 16. Trained disturbance No 14: reactive power response of the reduced system compared to the time-varying confidence interval (Q_5, Q_{95})

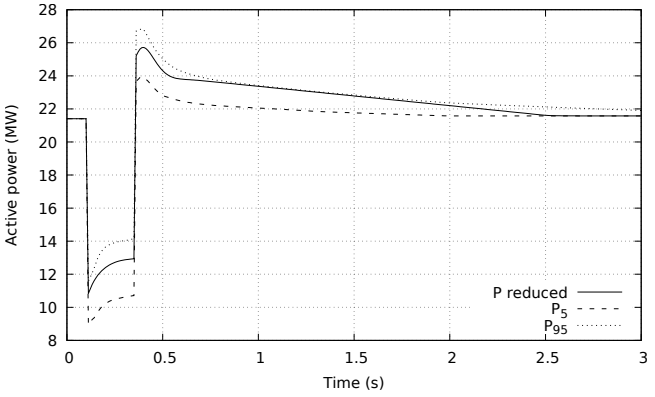

Fig. 17. Untrained disturbance No 6: active power response of the reduced system compared to the time-varying confidence interval (P_5, P_{95})

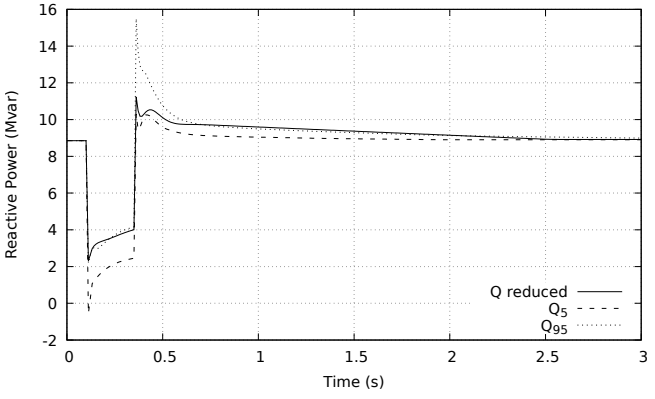

Fig. 18. Untrained disturbance No 6: reactive power response of the reduced system compared to the time-varying confidence interval (Q_5, Q_{95})

MC simulations of disturbances No 2 and 6. It is observed that the equivalent matches the confidence interval with the same satisfactory accuracy as for the trained disturbances.

VI. Summary and Perspectives

The ongoing research reported in this paper made up of two parts.

The first part consists of dealing with the uncertainty affecting the detailed, unreduced model of the ADN. It is assumed that the individual behaviour of IBGs and loads is reasonably well captured by a parameterized model, but the values of its parameters are uncertain. Monte-Carlo simulations involving random variations of those parameters are performed. The variables of interest are the active and reactive powers entering the ADN. The MC simulations are stopped once sufficient

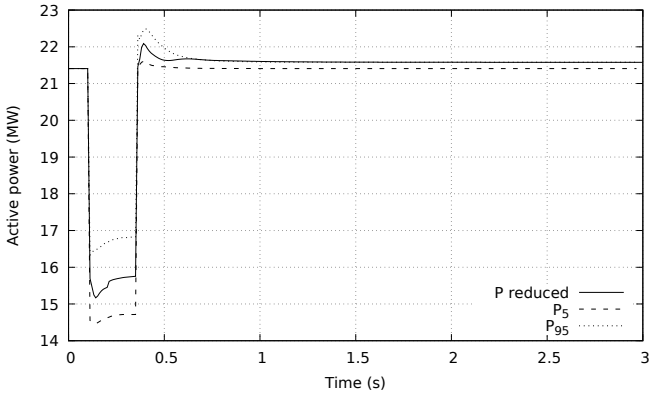

Fig. 19. Untrained disturbance No 2: active power response of the reduced system compared to the time-varying confidence interval (P_5, P_{95})

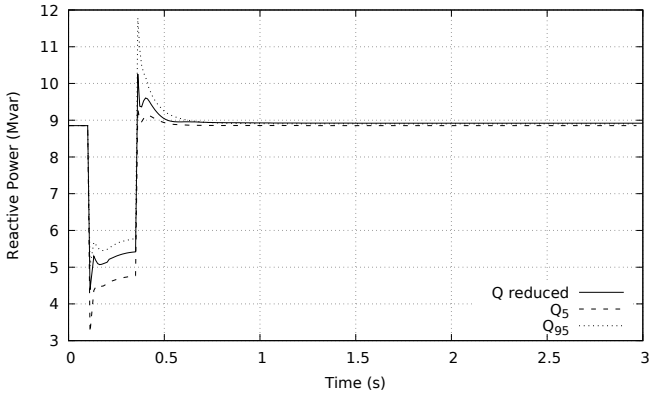

Fig. 20. Untrained disturbance No 2: reactive power response of the reduced system compared to the time-varying confidence interval (Q_5, Q_{95})

information is available. For each disturbance of interest, time-varying confidence intervals are extracted from the set of randomized time responses. Their bounds correspond to the 5-th and the 95-th percentiles of the distribution of dynamic responses at each discrete time.

The second part deals with the tuning of the parameters of a "grey-box" dynamic equivalent. The objective is to have its responses falling in the time-varying confidence intervals.

Results obtained from a CIGRE benchmark system show that the obtained equivalent can meet this objective, is accurate and not subject to overfitting.

The following extensions are among those envisaged in the near future.

- A wider range of training signals will be considered, including for instance phase jumps and frequency variations. The main motivation is to avoid "overfitting" particular training signals and make the equivalent suitable for a wider range of transients likely to take place in the transmission system. It has to be checked that this is not detrimental to accuracy.
- The training of the equivalent has been performed for a single operating point. A further step is to assess its accuracy for different operating points, corresponding to load levels and changing weather conditions affecting the renewable energy sources feeding the IBGs. Clearly, if a significant decrease of accuracy is experienced, the equivalent has to be updated for the new operating conditions. It is hoped that a limited number of parameter vectors will be enough to capture a wide range of operating points.
- The subset of disturbances selected for training was based on engineering judgment. Instead, a recursive algorithm is being developed to progressively select more and more training signals until the remaining are found to bring no further accuracy.
- Alternatives to the barrier function – see Fig. 2 and Eqs. (4-6) – are contemplated with the objective of taking into better account the dispersion of the randomized dynamic responses provided by MC simulations.
- Other optimization techniques are considered as alternatives to the DE algorithm.

REFERENCES

[1] Milanović, Jovica (convener), "Modelling and aggregation of loads in flexible power networks," *Report of CIGRE WG C4.605*, 2014.

[2] Hatziargyriou, Nikos (convener), "Contribution to bulk system control and stability by distributed energy resources connected at distribution network," *IEEE PES Tech. Report PES-TR22*, 2017.

[3] C. Z. Mooney, *Monte carlo simulation*, vol. 116. Sage Publications, 1997.

[4] I. A. Hiskens, M. Pai, and T. Nguyen, "Bounding uncertainty in power system dynamic simulations," in *Power Engineering Society Winter Meeting, 2000. IEEE*, vol. 2, pp. 1533–1537, IEEE, 2000.

[5] G. Chaspierre, P. Panciatici, and T. Van Cutsem, "Modelling Active Distribution Networks under Uncertainty: Extracting Parameter Sets from Randomized Dynamic Responses," *Proc. 20th PSCC conference*, Dublin (Ireland), 2018, in press.

[6] E. Langford, "Quartiles in elementary statistics," *Journal of Statistics Education*, vol. 14, no. 3, 2006.

[7] K. Price, R. M. Storn, and J. A. Lampinen, *Differential Evolution - A Practical Approach to Global Optimization*. Springer, 2005.

[8] G. Chaspierre, P. Panciatici, and T. Van Cutsem, "Dynamic Equivalent of a Distribution Grid Hosting Dispersed Photovoltaic Units," *Proc. IREP' 17 Symposium*, Espinho (Portugal), 2017, in press.

[9] P. Kotsampopoulos, N. Hatziargyriou, B. Bletterie, and G. Lauss, "Review, analysis and recommendations on recent guidelines for the provision of ancillary services by Distributed Generation," *Proc. IEEE Intern. Workshop on Intelligent Energy Systems*, pp. 185–190, 2013.

[10] VDE-AR-N 4120, "Technical requirements for the connection and operation of customer installations to the high-voltage network (TCC High-Voltage)," pp. 1–123, January 2015.

[11] B. Weise, "Impact of k-factor and active current reduction during fault-ride-through of generating units connected via voltage-sourced converters on power system stability," *IET Renewable Power Generation*, vol. 9, no. 1, pp. 25–36, 2015.

[12] G. Chaspierre, P. Panciatici, and T. Van Cutsem, "Aggregated Dynamic Equivalent of a Distribution System hosting Inverter-based Generators," *Proc. 20th PSCC conference*, Dublin (Ireland), 2018, in press.

[13] S. Barsali *et al.*, *Benchmark systems for network integration of renewable and distributed energy resources*. CIGRE Task Force, 2014.

[14] C. Taylor, *Power System Voltage Stability*. Mc Graw Hill, EPRI Power Engineering Series, 1994.

[15] P. Aristidou, D. Fabozzi, and T. Van Cutsem, "Dynamic simulation of large-scale power systems using a parallel Schur-complement-based decomposition method," *IEEE Trans. on Parallel and Distributed Systems*, vol. 25, no. 10, pp. 2561–2570, 2014.